Full Paper

Surface and Interface Spectroscopy of High Explosives and Binders: HMX and Estane

Hackjin Kim

Department of Chemistry, Chungnam National University, Taejon 305-764 (Korea)

Alexei Lagutchev, Dana D. Dlott*

School of Chemical Sciences, University of Illinois at Urbana-Champaign, Urbana, IL 61801 (USA)

DOI: 10.1002/prep.200600017

Abstract

Vibrational sum-frequency generation spectroscopy (SFG) is used to characterize the surfaces of β-HMX single crystals and Estane polymer binder, as well as the HMX-Estane interface. SFG is a nonlinear vibrational spectroscopy that selectively probes vibrational transitions at surfaces and interfaces. On the HMX {011} surface, both CH- and NO_2-stretching transitions are observed. Compared to bulk HMX, the surface transitions are blueshifted and the splittings are larger. This effect is explained by surface HMX molecules having partially buried and partially free CH_2 and NO_2 groups. Estane is a diblock copolymer with both soft and hard segments. Comparison of Estane spectra with polymers having only the soft unit and with polymers having predominantly hard units indicate there is a preference for the hard unit on the surface. SFG spectra of the HMX-Estane interface show smaller splittings of the HMX CH-stretch transitions than at the HMX-air interface, because the partially free surface groups are buried in Estane.

Keywords: Plastic Bonded Explosive, HMX, Interface, Vibrational Spectroscopy, Estane

1 Introduction

In this work we use vibrational sum-frequency generation spectroscopy (SFG) to investigate the surfaces and interfaces of β-octahydro-1,3,5,7-tetranitro-1,3,5,7-tetrazine (β-HMX) single crystals and Estane® 5703 polymer (hereafter Estane). These materials are the primary constituents of the high-performance plastic bonded explosives (PBX) LX-14 (95.5% HMX + 4.5% Estane) and PBX-9501 (95% HMX and Estane combined with nitroplasticizer).

SFG has emerged as one of the most powerful techniques for studying vibrational transitions of molecules at surfaces and interfaces, especially buried interfaces [1–3]. In broadband multiplex SFG [4, 5], a broadband pulse in the vibrational infrared (IR) is combined with a narrowband visible pulse, and the emitted sum-frequency pulse is detected with a spectrograph and a CCD. As opposed to narrowband SFG, with the broadband technique an entire spectral region is probed with every laser shot. The coherent SFG signal is generated by third-order nonlinear optical processes, and the signal is enhanced by molecular vibrational resonances so features similar to the usual vibrational fingerprints are seen in SFG. Traditionally the two biggest problems with surface vibrational spectroscopy have been sensitivity and selectivity. The number of molecules at the surface is small, only a tiny fraction of the number of molecules in the bulk. SFG helps alleviate both problems. The combination of intense femtosecond pulses (typically 10 GW/cm^2), coherence (the signal is emitted and collected as a coherent beam), and the very high sensitivity of CCD detectors to visible photons generates adequate signals from many interfacial species. Since third-order processes vanish in centrosymmetric media, SFG possesses a remarkable property. At the interfaces of two centrosymmetric media, e.g. crystal-air, polymer-air or crystal-polymer, SFG process probes the interface only. For instance:

With a β-HMX crystal (HMX-air interface), SFG ignores the bulk HMX and probes only functional groups at the HMX surface.

With Estane polymer (Estane-air interface), SFG ignores the bulk Estane and probes only functional groups at the Estane surface.

With an HMX-Estane interface, SFG probes only the HMX and Estane functional groups at the interface.

HMX has the chemical formula $(CH_2{-}N{-}NO_2)_4$, and at the HMX surface, the methylene (CH_2) and nitro (NO_2) groups are unique. They have different geometries, different interactions and enhanced configurational freedom relative to functional groups in the bulk crystal. Estane is a polyester polyurethane block co-polymer consisting of alternating soft and hard segments [6]. During processing and manufacturing [7], either the soft or the hard segments might

* Corresponding author, e-mail: dlott@scs.uiuc.edu

segregate at the polymer-air interface, so the concentration of surface groups may differ significantly from the bulk [1]. As the polymer ages, the polymer surface structure and composition may change significantly as a result of phase separation possibly assisted by prolonged contact with an HMX surface.

Practical PBX materials have quite complicated structures. At present little is known about the details of molecular structures at PBX surfaces and interfaces. Atomic-force microscopy can be used to study solid-air interfaces of high explosives [8], but AFM does not discriminate between molecular functionalities and AFM cannot see buried interfaces such as a polymer-crystal interface. One may list quite a few reasons why a fundamental understanding of these buried interfaces might be important:

- The mechanical strength of PBX materials can be limited by adhesion between the crystalline and polymer phases. Adhesion results from molecular interactions at the interface.
- Impact initiation of PBX can be quite sensitive to the presence or absence of voids. The presence of a void is strongly dependent on the adhesion between crystals and binders.
- Combustion processes of PBX are largely interfacial, resulting from chemical reactions at solid-solid, solid-liquid or solid-gas interfaces.
- A better knowledge of surface structures and interactions may permit the design of molecular surfactants that promote stronger interactions between the crystalline materials and the polymer binder, which might enhance insensitivity to impact initiation.
- Similarly, molecular surfactants might be developed that bind preferentially to specific crystal faces. In conjunction with processes that partially align polymer chains such as extrusion or spin coating, a greater degree of control may be exerted over the orientation distribution of crystals. The orientation distribution may play a role in determining impact sensitivity, since some energetic crystals – particularly PETN – have a high degree of orientational sensitivity to impact [9].
- Conversion of insensitive β-HMX to undesirable impact-sensitive δ-HMX upon heating, and reconversion upon cooling, is known to be facilitated by the binder in PBX 9501 [10, 11]. The δ-to-β reconversion is believed to be assisted by interfacial contact between crystal and polymer. Aged binder materials lose adhesion to the crystalline HMX and retard δ-to-β reconversion [12].

In this paper we demonstrate, for the first time, the use of SFG spectroscopy to characterize the surfaces of crystalline energetic materials, polymer binders and the polymer-crystal interface. Specifically we demonstrate a spectroscopic technique that is sensitive to the structure of the buried interface between β-HMX and Estane. Although much of surface science is focused on model systems with clean well-characterized surfaces in ultrahigh vacuum, in this work we are looking at the actual components of practical formulations. For this reason there are variations in the surface SFG spectra that would not be expected for perfect surfaces. We try to make clear the extent of these variations, which should be regarded as an intrinsic feature of practical materials and real interfaces.

2 Experimental

2.1 SFG Spectroscopy

SFG is a well-known spectroscopic technique and the subject of several reviews [1, 3, 13, 14]. SFG is a three-photon process where simultaneous vibrational infrared and "visible" pulses are incident on the sample and a coherent sum-frequency signal is generated and detected. (The term "visible" pulse is a historical term; this pulse could be any wavelength and here it is in the near-IR region). A special case of SFG is second-harmonic generation (SHG), where the two incident pulses are the same frequency. SHG has previously been used to study the kinetics of the transition between centrosymmetric β-HMX and noncentrosymmetric δ-HMX [10, 11]. The SFG intensity I_{SFG} is proportional to the square modulus of the nonlinear polarization $\vec{P}_{SFG}$, which itself depends on the second-order nonlinear susceptibility $\chi^{(2)}$

$$I_{SFG} \propto \left|\vec{P}_{SFG}\right|^2 = \left|\chi^{(2)}\vec{E}_{vis}\vec{E}_{IR}\right|^2 \tag{1}$$

where $\vec{E}$ denotes an electric field. The symmetry properties of $\chi^{(2)}$ lead to the well-known result that (in the dipole approximation) no SFG signal can be generated in centrosymmetric media [2]. It is difficult to calculate $\chi^{(2)}$ from molecular properties, but $\chi^{(2)}$ is often expressed in the form

$$\chi^{(2)}(\omega) = \chi^{(2)}_{NR} + \chi^{(2)}_{R} = \chi^{(2)}_{NR} + \sum_{v} \frac{NA_v}{\omega - \omega_v + i\Gamma_v} \tag{2}$$

In Eq. (2), $\chi^{(2)}$ is divided into nonresonant and resonant contributions. The nonresonant contribution in the near-IR for dielectric materials such as HMX and Estane is typically small and approximately independent of frequency over the typical range of frequencies of an SFG spectrum. The resonant contributions are expressed as a sum of Lorentzian lineshape functions where N is the number density, A_v an amplitude factor that is related to the IR and Raman cross-sections, ω_v is the IR frequency and Γ_v is the Lorentzian linewidth. Substituting Eq. (2) into Eq. (1) shows that for weak nonresonant contributions, an SFG spectrum should appear as a series of peaks located at the frequencies of molecular vibrational transitions [2, 3] that are both IR and Raman active. In a centrosymmetric medium, the only such transitions are associated with molecular moieties at a surface or interface.

In SFG, each of the three photons has two possible polarization states, so there are eight possible polarization combinations. The susceptibility $\chi^{(2)}$ is a third-rank tensor

with 27 elements but only 4 of these are independent [1]. The most common polarization condition for SFG has all three photons polarized in the plane of incidence, denoted *ppp*. The *ppp* spectrum is rich in spectral features, since all four independent elements of $\chi^{(2)}$ contribute to I_{SFG}. Another polarization combination that has proven especially useful for polymers [1] has the SFG signal polarized parallel to the plane of incidence, but the two incident photons are perpendicular to this plane (*ssp* polarization). The *ssp* signal arises from only one element of the $\chi^{(2)}$ tensor, $\chi^{(2)}{}_{yyz}$ [1], so this combination often produces the simplest spectra.

Our experiments utilize the broadband multiplex SFG technique [15]. The infrared pulse is a broadband femtosecond pulse, and the visible pulse is a picosecond narrowband 804 nm pulse. These pulses are incident on the sample at a 60° angle, and the SFG signal is detected with a spectrograph and multichannel CCD detector. The width of the visible pulse determines the spectral resolution, and here that resolution is 4 cm^{-1}. The center frequency Ω of the IR pulse and its fwhm (full width at half maximum) Δ (here $\Delta \approx 250\ cm^{-1}$) determines the IR spectral region being probed. To account for the variation of IR pulse intensity across this spectral region, we can approximate the pulse spectrum as a Gaussian (e. g. see the dashed spectrum in Figure 2) to give an analytical expression that is a good representation of our SFG spectra [16],

$$I_{SFG}(\omega) \propto \exp\left[-4\ln(2)\frac{(\omega-\Omega)^2}{\Delta}\right] \times \left|A_{NR}\exp(-i\phi)+\sum_{\nu}\frac{NA_{\nu}}{\omega-\omega_{\nu}+i\gamma_{\nu}}\right|^2 \quad (3)$$

where ϕ is the phase difference between the resonant and nonresonant contributions.

A block diagram of the laser apparatus, described elsewhere in more detail [17], is shown in Figure 1. An amplified femtosecond Ti:Sapphire laser (Kapteyn-Murnane oscillator and Quantronix Titan amplifier) generated 804 nm pulses of 100 fs duration at 1 kHz [15]. Most of the ~ 2 mJ laser pulse pumps an optical parametric amplifier (Light Conversion, TOPAS DFG), which generates femtosecond IR pulses that can be tuned through the 2.5 to 16 μm range. The remaining 804 nm (visible) pulse is spectrally filtered to 4 cm^{-1} fwhm using a Fabry-Perot étalon. The IR and visible beams are combined with a dichroic beamsplitter and focused onto the sample to a spot size of ~ 200 μm diameter. A short pass filter (Omega Optical) cuts out the visible light at 804 nm and transmits the SFG signal, which is centered near 644 nm for CH-stretch and near 720 nm for NO_2-stretch transitions. The SFG signal is detected with a 0.5 m Chromex spectrograph and an Andor CCD detector. Typical displayed spectra were the result of signal acquisitions for five minutes.

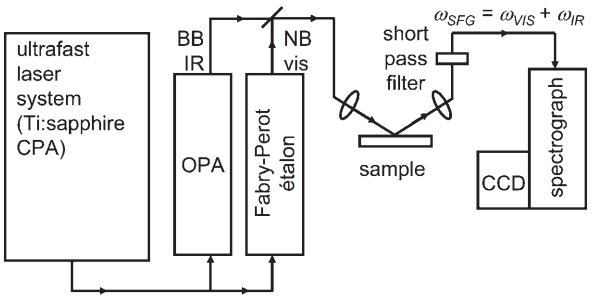

Figure 1. Block diagram of the laser system. CPA = chirped-pulse amplifier. OPA = optical parametric amplifier. BBIR = broad-band infrared pulse. NBvis = narrow-band visible pulse.

2.2 Materials

HMX and Estane 5703 were provided by Dr. Randall Simpson and Dr. George Overturf of the Energetic Materials Center, Lawrence Livermore Laboratory. Additional samples of HMX were provided by Dr. Dan Hooks of Los Alamos National Laboratory. HMX single crystals were grown from acetone solution, and as expected the largest crystal face was parallel to {011}. The spectra shown here were obtained from this {011} face of a crystal, approximately $5 \times 2 \times 1\ mm^3$. The crystal was oriented using X-ray diffraction. Infrared spectra were obtained with HMX in a KBr pellet, which provides an average over all orientations, using a Nicolet 760 FT-IR spectrometer.

Estane was dissolved in methyl ethyl ketone and spin-coated on a sapphire substrate. Sapphire was used because it could be thoroughly cleaned with strong acid to remove all surface oils. Some Estane samples were baked in vacuum at 100 °C. Given the variability in the Estane SFG spectra, baking had no significant effect. In addition to Estane, we used two model polymers to help assign the Estane vibrational spectrum.

The Estane monomer has the form

$$[(CH_2)_4COO(CH_2)_4COO]_m - [O(CH_2)_4 OCONH{-}Ph{-}CH_2{-}Ph{-}NH{-}COO]_n$$

where Ph (phenyl) denotes C_6H_4, *m* is typically 4 – 6 and *n* is typically 1 – 3.

The polymer poly-(1,4-butylene adipate) (PBA) was obtained from Aldrich and samples were prepared as with Estane. The PBA polymer consists entirely of the soft segments of Estane having the structure

$$[(CH_2)_4COO(CH_2)_4COO]_n$$

The hard polyurethane segments do not form a polymer by themselves, so we used a polymer that consists of a short soft chain extender 1,4-butanediol (BDO) linked to the hard urethane segment 4,4′-diphenylmethane diisocyanate (MDI). The structure of BDO/MDI polymer is

$$[O(CH_2)_4OCONH{-}Ph{-}CH_2{-}Ph{-}NH{-}COO]_n$$

The BDO/MDI was synthesized using methods described in Ref. [6]. This polymer was dissolved in dimethyl formamide solvent and spin-coated onto sapphire.

3 Results

3.1 HMX {011}-Air Interface

Figure 2 shows SFG spectra of the {011} face of a solution-grown HMX crystal, in the CH-stretch region, with *ppp* and *ssp* polarizations. The dashed curve is the SFG signal from a gold surface, which gives the apparatus spectral response, which was discussed above in connection with Eq. (3). The laser beams scanned the {011} surface of an HMX crystal, and variations were observed in the spectra with position. The laser beams sample regions ~ 200 μm in diameter. Since the spectra arise in principle from a surface monolayer of HMX, the total amount of material contributing to the signal is $\sim 4 \times 10^{10}$ molecules or ~ 20 pg. The different rows in Figure 2 are spectra from different locations that were deemed representative.

Figure 3 compares the FT-IR spectrum in the CH-stretch region of bulk HMX (powder) to SFG spectra of a single crystal that could be rotated about an axis perpendicular to {011}. The FT-IR spectrum consists of a pair of doublets. As discussed below, the larger splitting of $\sim 40\ cm^{-1}$ is the $\nu_s(CH_2)$-$\nu_a(CH_2)$ splitting [18, 19], and the smaller splitting of $\sim 10\ cm^{-1}$ is the factor-group splitting resulting from two molecules per unit cell [20 – 22]. β-HMX belongs to the P_{21}/c space group and the unit cell has C_{2h} symmetry. Transitions are polarized either parallel to the *b*-axis (the symmetry axis) or perpendicular to the *b*-axis (i. e. in the *ac* plane) [20]. The crystal rotation spectra in Figure 3 show that the two components of each doublet are polarized either parallel to the *b*-axis or perpendicular to the *b*-axis, confirming that this smaller splitting is a factor-group splitting in the C_{2h} group.

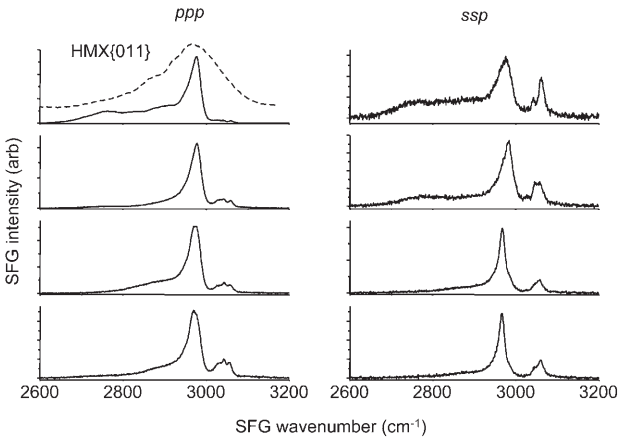

Figure 2. Vibrational sum-frequency generation (SFG) spectra of the {011} face of an HMX crystal in the CH stretch region. The dashed curve represents the apparatus spectral response. Each row of the figure indicates SFG spectra from different locations on the crystal face obtained in ppp and ssp polarizations.

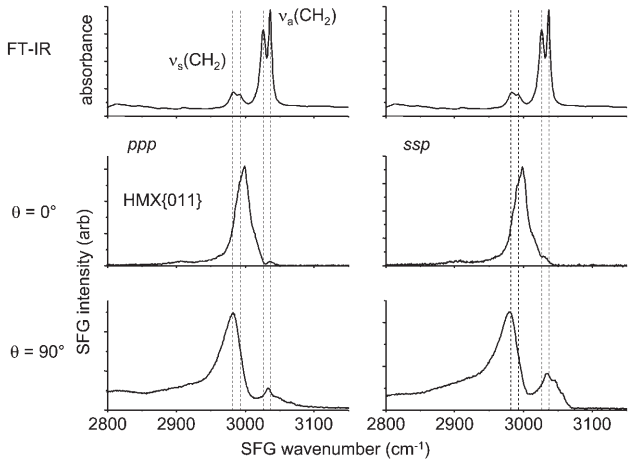

Figure 3. Comparison of the FT-IR and SFG spectra of HMX. The FT-IR (powder) spectrum consists of a pair of doublets representing the $\nu_s(CH_2)$ and $\nu_a(CH_2)$ transitions. The doublet structure is due to the factor-group splitting. The SFG spectrum of the {011} face also consists of a pair of doublets. Rotation of the crystal shows the doublets have one peak polarized parallel to the unique *b*-axis and one perpendicular to this axis. On the surface the peaks are blueshifted and the splittings are larger.

Comparing the SFG spectra of surface HMX to FT-IR spectra of bulk HMX shows that the CH-stretch transitions on the surface are generally blueshifted and the splittings are larger than in the bulk. At some locations on the variable surface minor peaks with even larger blueshifts were seen.

Figure 4 shows HMX spectra in the NO_2-stretch region. The FT-IR spectra of bulk HMX shows intense transitions at $\sim 1280\ cm^{-1}$ and $\sim 1560\ cm^{-1}$, which correspond to the $\nu_s(NO_2)$ and $\nu_a(NO_2)$ transitions. Each of the major FT-IR peaks evidences unresolved multiplet structure; at least two major subpeaks are evident. As in the CH-stretch region, the SFG spectra varied somewhat with location on the crystal surface, and spectra from two surface locations are shown that are representative of this variability. The SFG spectra show well-resolved doublet structure for both the $\nu_s(NO_2)$ and $\nu_a(NO_2)$ transitions. As in the CH-stretch region, relative to the bulk spectrum, the NO_2-stretch peaks are blueshifted and the splittings are larger. However the NO_2-stretch linewidths are somewhat smaller than in the bulk.

3.2 Estane-Air Interface

Figure 5 shows SFG spectra of Estane, PBA and MDI/BDO, along with FT-IR spectra in the CH-stretch region. The polymer spectra also showed position-dependent variability. The spectra displayed here, two different polarization conditions at two different locations, were judged representative. The spectra are structured but poorly resolved. The peaks seen in the pure PBA spectrum (soft segments only) in the CH-stretch region were labeled A – D. Two peaks in MDI/BDO (hard segments plus short soft linkers) not present in PBA were labeled E and Ph–H, and these were assigned to the functional units not present in

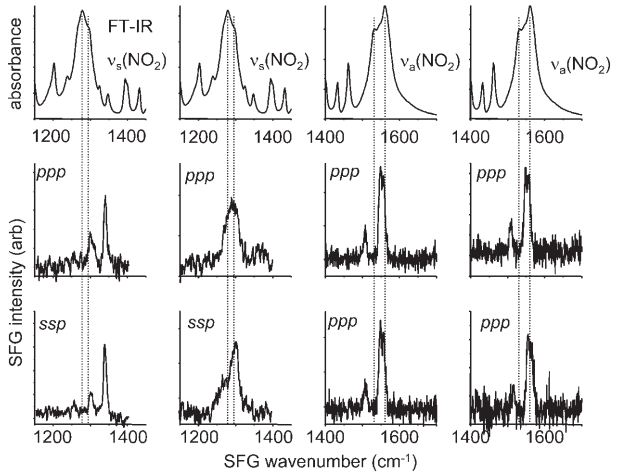

Figure 4. FT-IR and SFG spectra of HMX in the NO_2-stretch region consists of a pair of doublets due to $\nu_s(NO_2)$ and $\nu_a(NO_2)$. The second and third rows are SFG spectra obtained at two different locations on the {011} surface.

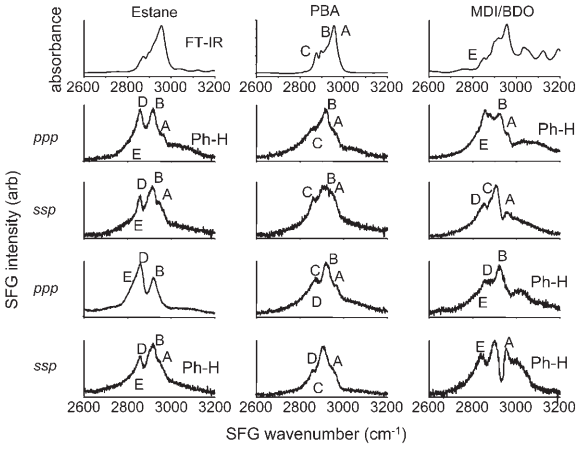

Figure 5. Spectra of Estane, PBA and MDI/BDO polymers. The PBA polymer consists of the soft segments of Estane only. MDI/BDO consists of the hard segments plus short soft segment linkers. Peaks A – D identify CH-stretching transitions of the soft segments. Redshifted peak E identifies CH-stretch transitions of the linker group Ph–CH_2–Ph (Ph = phenyl = $-C_6H_4-$) and the blueshifted CH-stretch transitions of the phenyl groups. Rows 2 – 3 and 4 – 5 represent different spots on the polymer surfaces.

PBA. The redshifted peak labeled E corresponds to CH-stretch transitions of the methylene linker group Ph–CH_2–Ph, and Ph-H corresponds to CH-stretch transitions of the urethane phenyl groups, which are blueshifted from methylene transitions by ~ 100 cm^{-1}.

Figure 6 shows an SFG spectrum of a fresh Estane surface and of the same spot on the surface after it was touched with a latex glove. A new sharp peak appears near 2950 cm^{-1}. A similar peak was seen if the Estane was touched with a bare finger or a piece of Teflon tape. However if the Teflon tape was washed in an organic solvent and then dried in a vacuum oven before touching the Estane surface, this peak was not observed. The peak is associated with minute quantities of oils that are present on all surfaces in the laboratory.

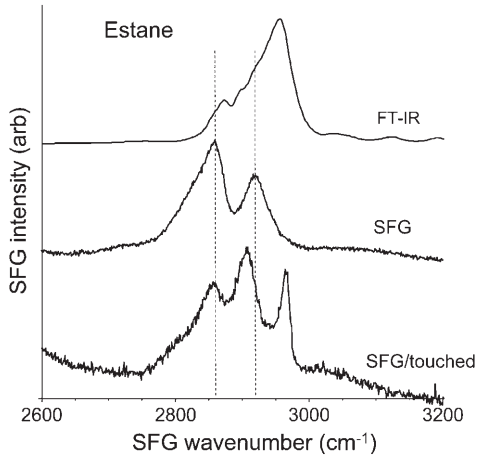

Figure 6. Touching the Estane surface with a latex glove, a fingertip or a piece of Teflon tape generates a sharp new peak near 2950 cm^{-1} attributed to oil on the Estane surface. If the Teflon tape is cleaned and baked first, this peak does not appear.

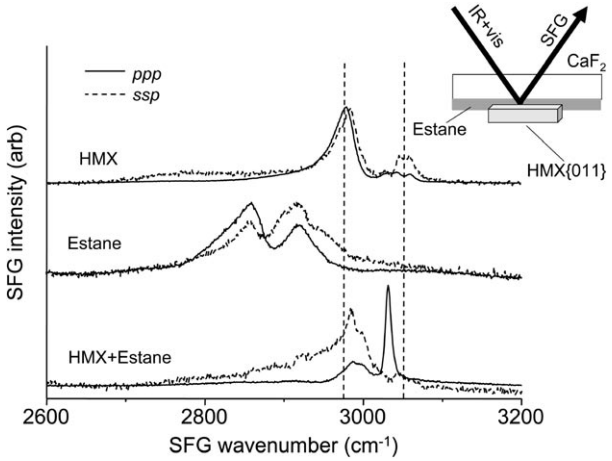

Figure 7. SFG spectra at the HMX-Estane interface obtained using the arrangement shown at upper right is compared to SFG spectra of pure HMX or pure Estane.

Figure 7 shows an SFG spectrum obtained at the Estane-HMX interface. A CaF_2 window was coated with a thin layer of Estane, which was brought into contact with the {011} surface of an HMX crystal. The results with this arrangement could be quite variable because the polymer-crystal contact was imperfect. The spectrum displayed in Figure 7 is one that clearly shows the HMX transitions through the Estane layer, and a comparison with the HMX SFG spectrum shows that the splitting between the $\nu_a(CH_2)$ and $\nu_s(CH_2)$ peaks of HMX decreases in contact with Estane.

4 Discussion

4.1 Spectroscopy of HMX Crystal and Surface

Here a brief discussion of crystal vibron spectroscopy is presented that allows us to qualitatively explain the shifts

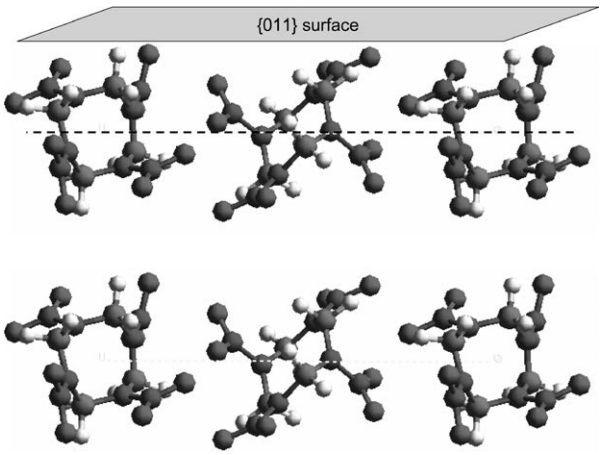

Figure 8. Molecular structure of the HMX {011} surface. Each molecule on the surface has one partially buried NO_2 and CH_2 group and one partially free group.

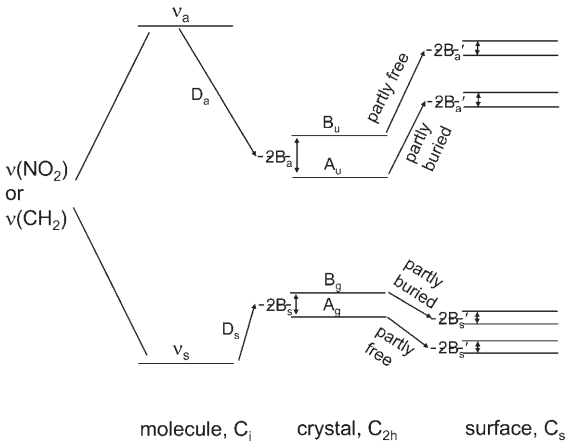

Figure 9. Correlation diagram for HMX crystal and surface. *D* represents the gas-to-crystal shift. 2*B* represents the factor-group splitting. The primed quantities are the gas-to-surface shift and the surface factor-group splitting.

and splittings observed for HMX surface vibrations. An isolated HMX molecule has C_i symmetry in the chair configuration found in β-HMX [18, 19]. Each HMX molecule has four pairs of CH-stretch or NO_2-stretch transitions, but for simplicity we consider just one pair of $\nu_s(CH_2)+\nu_a(CH_2)$ or $\nu_s(NO_2)+\nu_a(NO_2)$ bands. This simplification is justified for the present discussion because due to our SFG sensitivity we see only the strongest band. These are transitions having the largest SFG hyperpolarizibilities, which are presumably ones where the methylene or nitro dipoles and polarizabilities add in-phase.

The gas-to-crystal vibrational frequency shift is conventionally designated *D*. The value of *D* is different for every mode of vibration, and *D* may be positive or negative. The factor-group or Davydov splitting resulting from interactions between the two inequivalent molecules is conventionally designated 2*B*. One expects $|2B|<|D|$, since *D* results from interactions with *every* other molecule whereas *2B* results from interactions with *inequivalent* molecules only. The {011} surface is a 2-dimensional lattice with two inequivalent molecules per unit cell. We expect the magnitudes of the gas-to-surface shift D' and the factor-group splitting $2B'$ to be smaller than *D* and 2*B,* since on the surface each molecule interacts with one-half as many other molecules. (Keep in mind these are just general considerations rather than hard and fast rules, since surface reconstruction and specific interactions among surface molecules might cause different results in some cases.)

Figure 8 is a drawing of the molecules at the HMX {011}-air interface, constructed using the Cerius[2] molecular modeling package. In this figure we are looking down the *a*-axis and the {011} plane is perpendicular to the page. At the surface, each molecule has two inequivalent NO_2 and two inequivalent CH_2 groups. The inequivalent groups lie approximately parallel or perpendicular to the plane. Based on this drawing, we will term the NO_2 and CH_2 groups perpendicular to the plane as "partially buried" and the parallel groups as "partially free". The magnitude of D′ for the partially buried functional groups is expected to be larger (i.e. closer to the bulk value) than for the partially free groups.

Figure 9 is a correlation diagram for bulk and surface HMX molecules that is appropriate for both CH_2 and NO_2 stretch transitions. We used the calculated frequencies from Brand et al. [18] of the most intense transitions of an HMX isolated molecule in the C_i configuration for the gas-phase reference. Then we found the gas-to-crystal shift D_a for the ν_a modes to be negative (gas-to-crystal redshift) and D_s for the ν_s modes to be smaller and positive. The surface levels were drawn assuming that $|D|>|D'|$(partially buried) $>|D'|$(partially free) and that $|2B|>|2B'|$as discussed above.

4.2 Interpretation of HMX Surface Spectra

In comparing the HMX crystal spectra with the HMX {001} surface spectra, we noted that on the surface the peaks were blueshifted and the splittings were larger. These observations seemingly contradict our expectation that the factor-group splittings should be smaller on the surface. Figures 8 and 9 provide an explanation of these results. The splittings seen in the SFG spectra do not result from the factor-group effect, but instead represent differences in the gas-to-surface shift between the partly-buried and partly-free CH_2 and NO_2 groups. The energy splitting between partly-buried and partly-free groups is larger than the factor-group splitting.

4.3 Estane SFG Spectra

SFG studies of polymers have been recently reviewed [1]. There are several cases where the polymer surface spectrum is noticeably different from the bulk. Estane is, we believe, the first diblock copolymer studied by SFG which raises the

question as to whether the surface composition differs significantly from the bulk and if one of the two components, hard or soft, is more likely to predominate at the surface. It is known that when the bulk polymer ages, the urethane segments tend to phase-separate and form interchain hydrogen bonds, which can be detected with FT-IR via the interchain hydrogen bonding [23, 24]. Here we look at the question of whether there is SFG evidence for phase segregation at the Estane surface.

The soft segments of Estane are characterized by a preponderance of CH_2 groups due to the butane $(CH_2)_4$ moieties, and the peaks labeled A – D in the PBA spectra (Figure 5) are indicators that soft segments are on the surface. The MDI/BDO polymer has both hard and soft segments, but the hard segments have two unique identifiers that can be seen by comparing the PBA and MDI/DBO spectra in Figure 5. These are the peaks labeled E, which represent the redshifted CH-stretch transitions from the methylene linker Ph-CH_2-Ph, and the blueshifted Ph-H stretch transitions. Thus in the SFG spectra of Estane, we should look at the ratio of soft (butane) to hard (Ph–CH_2–Ph and Ph–H) transitions. In Figure 5 the SFG spectra from Estane are variable, but even taking the variability into account they appear to have quite a bit more of the peak denoted E as well as the Ph–H transitions than does the bulk FT-IR spectrum. This observation indicates a degree of phase segregation, with the hard segments congregating preferentially on the surface.

4.4 Estane-HMX Interface

So far, obtaining reproducible spectra of the Estane-HMX interface has been difficult because the contact region between the two materials is variable. As we scan the laser beam across the sample in the arrangement portrayed in Figure 7, we see changing contributions of Estane and HMX. The spectrum displayed in Figure 7 is not representative, but it is a spectrum where significant Estane and HMX contributions were observed simultaneously. In Figure 7 we see a sharp HMX transition in the *ppp* spectrum that is redshifted and does not show the splitting seen at the air-HMX interface. This observation is consistent with our attribution of the splitting in the SFG spectrum of the HMX-air interface as arising from the different energies of partially free and partially buried CH_2 species. At an Estane interface, functional groups that are partially free in air are now buried in Estane, resulting in a decrease in this splitting.

5 Summary and Conclusion

Interactions between crystal surfaces and polymer binders can play an important role in the behavior of PBX materials. By the standards of surface science, where a great deal of effort is expended to study perfectly clean well-characterized surfaces in ultrahigh vacuum, surfaces and interfaces in energetic materials are buried and dirty. The crystals are grown from solution, and when a crystal is removed from solution, rapid drying of the solution contaminates the crystal faces. This contamination is the most likely cause of the nonreproducibility we observe in scans across the {001} planes. The binders used in PBX are mixed with a variety of plasticizers and are heavily worked over with various mixing and casting devices during material processing. As shown in Figure 6, simply touching a fresh Estane surface with almost any kind of material transfers a thin layer of oil to the surface.

Nonetheless we have made a strong case for the use of SFG spectroscopy to probe these dirty, buried, but technologically important, interfaces. Although our SFG spectra are not entirely reproducible, some seemingly reliable interpretations can be made based on observations at several locations on the surface. New splittings are seen in the CH-stretch and NO_2-stretch region of HMX, which are caused by partially buried and partially free functional groups. The Estane surface appears to have a greater contribution of the hard component of the block copolymer than the Estane bulk. At the Estane-HMX interface, the differences between partially buried and partially free functional groups are reduced. A great deal of work remains in order for us to fully understand this type of interface, but this preliminary study representing the first application of surface spectroscopy to interfaces found in PBX materials has been extremely encouraging.

6 References

[1] Z. Chen, Y. R. Shen, G. A. Somorjai, Studies of Polymer Surfaces by Sum Frequency Generation Vibrational Spectroscopy, *Annu. Rev. Phys. Chem.* **2002**, *53*, 437.
[2] Y. R. Shen, Surface Properties Probed by Second-harmonic and Sum-frequency Generation, *Nature (London, U. K.)* **1989**, *337*, 519.
[3] Y. R. Shen, Surfaces Probed by Nonlinear Optics, *Surf. Sci.* **1994,** *299/300*, 551.
[4] L. J. Richter, T. P. Petralli-Mallow, J. P. Stephenson, Vibrationally Resolved Sum-frequency Generation with Broad-bandwidth Infrared Pulses, *Opt. Lett.* 1998, **23**, 1594.
[5] J. Patterson, A. S. Lagutchev, D. D. Dlott, Shock Compression of Molecules with 1.5 Angstrom Resolution, *13th Conference of the American Physical Society Topical Group on Shock Compression of Condensed Matter*, Portland, Oregon (USA), July 20 – 25, **2003**, AIP Conference Proc. 706, p. 1299.
[6] L. Cuvé, J. P. Pascault, G. Boiteux, G. Seytre, Synthesis and Properties of Polyurethanes Based on Polyolefine: 1. Rigid Rolyurethanes and Amorphous Segmented Polyurethanes Prepared in Polar Solvents under Homogeneous Conditions, *Polymer* **1991**, *32*, 343.
[7] D. J. Kasprzyk, D. A. Bell, R. L. Flesner, S. A. Larson, Characterization of a Slurry Process Used to Make a Plastic-bonded Explosive, *Propellants, Explos., Pyrotech.* **1999**, *24*, 333.
[8] J. Sharma, C. S. Coffey, R. W. Armstrong, W. L. Elban, S. M. Hoover, Sub-molecular Fracture Steps in Shock-shattered RDX Crystals and Follow-on Nano-indentation Evaluation of Early Stage Plasticity, *12th Conference of the American Physical Society Topical Group on Shock Compression of Condensed Matter,* Atlanta, Georgia (USA), June 24 – 29, **2001**, AIP Conference Proc. 620, p. 837.

[9] J. J. Dick, R. N. Mulford, W. J. Spencer, D. R. Pettit, E. Garcia, D. C. Shaw, Shock Response of Pentaerythritol Tetranitrate Single Crystals, *J. Appl. Phys.* **1991**, *70*, 3572.
[10] L. Smilowitz, B. F. Henson, M. Greenfield, A. Sas, B. W. Asay, P. M. Dickson, On the Nucleation Mechanism of the β-δ Phase Transition in the Energetic Nitramine Octahydro-1,3,5,7-tetranitro-1,3,5,7-tetrazocine, *J. Chem. Phys.* **2004**, *121*, 5550.
[11] L. Smilowitz, B. F. Henson, B. W. Asay, P. M. Dickson, The β-δ phase Transition in the Energetic Nitramine-octahydro-1,3,5,7-tetranitro-1,3,5,7-tetrazocine: Kinetics, *J. Chem. Phys.* **2002**, *117*, 3789.
[12] C. K. Saw, C. M. Tarver, Binder/HMX Interaction in PBX9501 at Elevated Temperatures, *13th Conference of the American Physical Society Topical Group on Shock Compression of Condensed Matter*, Portland, Oregon (USA), July 20 – 25, **2003**, AIP Conference Proc. 706, p. 1029.
[13] K. B. Eisenthal, Equilibrium and Dynamic Processes at Interfaces by Second Harmonic and Sum Frequency Generation, *Annu. Rev. Phys. Chem.* **1992**, *43*, 627.
[14] G. L. Richmond, Molecular Bonding and Interactions at Aqueous Surfaces as Probed by Vibrational Sum Frequency Spectroscopy, *Chem. Rev. (Washington, DC, U. S.)* **2002**, *102*, 2693.
[15] J. E. Patterson, A. Lagutchev, W. Huang, D. D. Dlott, Ultrafast Dynamics of Shock Compression of Molecular Monolayers, *Phys. Rev. Lett.* **2005**, *94*, 015501.
[16] G. Q. Lu, A. Lagutchev, D. D. Dlott, A. Wieckowski, Quantitative Vibrational Sum-frequency Generation Spectroscopy of Thin Layer Electrochemistry: CO on a Pt Electrode, *Surf. Sci.* **2005**, *585*, 3.
[17] A. S. Lagutchev, J. E. Patterson, W. Huang, D. D. Dlott, Ultrafast Dynamics of Self-Assembled Monolayers Under Shock Compression: Effects of Molecular and Substrate Structure, *J. Phys. Chem. B* **2004**, *109*, 5033.
[18] H. V. Brand, R. L. Rabie, D. J. Funk, I. Diaz-Acosta, P. Pulay, T. K. Lippert, Theoretical and Experimental Study of the Vibrational Spectra of the α, β, and δ Phases of Octahydro-1,3,5,7-tetranitro-1,3,5,7-tetrazocine (HMX), *J. Phys. Chem. B* **2002**, *106*, 10594.
[19] J. L. Lyman, Y.-C. Liau, H. V. Brand, Thermochemical Functions for Gas-phase, 1,3,5,7-Tetranitro-1,3,5,7-tetraazacyclooctane (HMX), its Condensed Phases and its Larger Reaction Products, *Combust. Flame* **2002**, *130*, 185.
[20] M. Suzuki, T. Yokoyama, M. Ito, Polarized Raman Spectra of Naphthalene and Anthracene Single Crystals, *Spectrochim. Acta, Part A* **1968**, *24*, 1091.
[21] A. S. Davydov, *Theory of Molecular Excitons,* The Maple Press Co., York, PA, **1962**.
[22] S. Califano, V. Schettino, N. Neto, *Lattice Dynamics of Molecular Crystals,* Springer-Verlag, Berlin, **1981**.
[23] J. R. Schoonover, D. G. Thompson, J. C. Osborn, E. B. Orler, D. A. Wrobleski, A. L. Marsh, H. Wang, R. A. Palmer, Infrared Linear Dichroism Study of a Hydrolytically Degraded Poly-(ester urethane), *Polym. Degrad. Stab.* **2001**, *74*, 87.
[24] H. Wang, S. R. Aubuchon, D. G. Thompson, J. C. Osborn, A. L. Marsh, W. R. Nichols, J. R. Schoonover, R. A. Palmer, Temperature-dependent Dynamic Mechanical Analysis-Fourier Transform Infrared Study of a Poly(ester urethane) Copolymer, *Macromolecules* **2002**, *35*, 8794.

Note added in proof: We have shown that most of the non-reproducibility in the β-HMX surface spectra stems from tiny amounts of δ-HMX on the surface. δ-HMX is noncentrosymmetric, and all the molecules in the δ-HMX crystallites contribute to the SFG signal (see Section 3.1).

Acknowledgements

This material is based on work supported by the U.S. Department of Energy through the Stewardship Sciences Academic Alliance Program from the Carnegie-DOE Alliance Center under Award No. DE-FC03-03NA00144 and the Frederick Seitz Materials Research Laboratory and the Center for Microanalysis of Materials at the University of Illinois at Urbana-Champaign under Award No. DEFG02-91ER45439. Additional support was provided by the US Air Force Office of Scientific Research under award number F49620-03-1-0032 and by the US Army Research Office under contract W911NF-05-1-0345. We thank Dr. Randall Simpson and Dr. George Overturf of the Energetic Materials Center, Lawrence Livermore Laboratory and Dr. Dan Hooks of Los Alamos National Laboratory for providing samples and for providing much useful information about these materials.

(Received: July 9; 2005; Ms 2005/123)

